Research Square

Preprints are preliminary reports that have not undergone peer review.
They should not be considered conclusive, used to inform clinical practice,
or referenced by the media as validated information.

Modelling the Suspended Sand Concentration Profile Under Breaking Waves

Gabriel Lim
University of East London
Nilakshan Balasubramaniam
University of East London
Mohammad Tabasi
Fudo Tetra (Japan)
Ravindra Jayaratne
r.jayaratne@uel.ac.uk

University of East London

Research Article

Keywords: reference concentration, suspended sand concentration, breaking waves, concentration profile, near-shore, turbulent kinetic energy

Posted Date: June 23rd, 2026

DOI: https://doi.org/10.21203/rs.3.rs-9873851/v1

License: This work is licensed under a Creative Commons Attribution 4.0 International License.
Read Full License

Additional Declarations: No competing interests reported.

MODELLING THE SUSPENDED SAND CONCENTRATION PROFILE UNDER BREAKING WAVES

First Author: Gabriel Lim[a]

Second Author: Nilakshan Balasubramaniam[b]

Third Author: Mohammad Tabasi[c]

Fourth Author (Corresponding): Ravindra Jayaratne[d*]

[a,b,d]Department of Engineering & Construction, University of East London, Docklands Campus, University Way, E16 2RD, London, UK. [a]gab91@hotmail.co.uk, [b]nilakshan@uel.ac.uk, [d]r.jayaratne@uel.ac.uk,

[c]Technical Research Institute, Fudo Tetra Corporation, Tsuchiura, Ibaraki, Japan.

[c]tabasi.mohammad@fudotetra.co.jp

ABSTRACT

Five suspended sand concentration profile [C(z)] models, four existing formulations and one modified model, were evaluated against 119 laboratory tests from four large-scale datasets covering multiple cross-shore zones under regular and irregular breaking waves. Existing formulations were grouped into power-law and exponential models, producing mildly parabolic and quasi-linear profiles, respectively. The classical Rouse profile was found unsuitable near the bed and free surface, yielding unrealistic concentrations as $z \rightarrow 0$ and $z \rightarrow d$, and therefore recommended only when the local water depth greatly exceeds reference elevation. Power-law models derived from the Rouse formulation exhibited excessively steep profiles due to small mixing parameter values, leading to quasi-uniform concentrations throughout the water column. In contrast, measured profiles were consistently concave, with elevated near-bed concentrations and reduced values in the upper water column, resulting in substantial overprediction by power-law models aloft. To address this limitation, a physics-

based correction factor was introduced to enhance the mixing parameter, producing a modified SR93-based formulation [L19 C(z)] that yields more realistic, smoothly varying profiles. The L19 model demonstrated superior agreement with observations across all cross-shore zones, with root-mean-square errors ranging from 0.03 to 2.3 kg m^{-3} (mean 0.56 kg m^{-3}), outperforming existing models. Exponential formulations reproduced concentrations near the bed and surface but diverged in the mid-water column and were highly sensitive to reference concentration specification. Finally, the L19 model was validated within a process-based morphodynamic framework using field data from the Hasaki Oceanographic Research Station, achieving a Brier Skill Score of 0.72 under storm conditions.

Keywords: reference concentration, suspended sand concentration, breaking waves, concentration profile, near-shore, turbulent kinetic energy

1. Introduction

Coastal morphodynamics is a product of small- and large-scale processes that occur over long (decadal +) time scales. As these processes are non-linear, occur over large areas (in the 10 to 100 km) over many years (10 to 100 years), they are difficult to predict. Process-based models (e.g. Delft3D) simulate waves, currents, sediment transport, and morphology together. By using tools such as MORFAC (morphological acceleration) and input reduction, modern models now simulate longer-term beach evolution. However, limitations in transport formulae remain (e.g. Wang et al., 2014; van der Wegen & Roelvink, 2008; Dastgheib, 2012; Sanchez et al., 2015; Dam et al., 2016; Luijendijk et al., 2019). Consequently, modellers are often forced to rely on arduous and time-consuming calibration efforts and practical models, which sometimes consist of (numerous) empirical tuning constants, to obtain favourable model results. Even state-of-the-art coastal area models such as Delft3D, MIKE21 and Telemac are comprised of relatively simple physics, relying instead on numerous (semi-) empirical parameterisations which are often not very well-founded in measured data nor on fundamental understanding of key hydrodynamic and sediment transport processes (van der Werf et al., 2015). Of the models that are thoroughly validated against experimental data, many are only validated for their ability to predict bed changes, rather than individual bedload and suspended load components (Van der Zanden et al., 2017a) and their relative contributions to net transport. Such methods and models are therefore often quite crude and/or inefficient but somewhat unavoidable due to theoretical limitations of existing models. An essential first step in improving morphodynamic modelling capabilities is the development of more robust sediment transport formulae that are accurate, widely applicable (to a range of different conditions) and computationally efficient. There is therefore a need for the development of more improved (practical and process-based) sediment transport formulae that are well-validated against data from field and laboratory experiments (van Rijn et al., 2013). This is especially the case for the

47 breaking and swash zones where previous attempts at accurately modelling the suspended
48 sediment transport have been most challenging due to the complex interaction between highly
49 turbulent hydrodynamic processes and transported sediments that occur in these regions (c.f.
50 Van der Zanden, 2016). Such processes include vertical (Van der Zanden et al., 2019) and
51 cross-shore (van Rijn et al., 2013; Van der Zanden et al. 2017b) hydrodynamic non-uniformity,
52 breaking induced turbulence and asymmetric oscillatory motion under shallow water waves
53 (Sato et al., 1990).

54 Lim et al. (2020) recently carried out an extensive evaluation study on the performance of six
55 existing reference concentration formulae against state-of-the-art high-resolution datasets
56 collected under prototype-scale regular and irregular breaking waves. It was reported that all
57 tested C_0 models produced large discrepancies particularly in the wave plunging region of the
58 breaking zone where the Suspended Sand Concentration (SSC) levels were highest. This was
59 attributed to the strong breaking-generated turbulent vortices which enhanced bed-shear
60 stresses and induced increased sediment pickup and vertical mixing. High-resolution large-
61 scale datasets consisting of sediment concentration measurements (with co-located
62 hydrodynamic and morphological data) carried out in numerous cross-shore locations were not
63 widely available until recent years. As a result, many of the existing SSC models (like the C_0
64 models evaluated by Lim et al., 2020) were only validated under a limited number of measured
65 cases in the breaking and shoaling zones, and often did not consider the effects of wave
66 breaking at all (van Rijn et al., 2013; Van der Zanden, 2016). In other cases, the models were
67 largely validated using data from small-scale wave flumes (e.g. Sato et al., 1990), where the
68 extent of hydrodynamic forces/processes found under field-scale breaking waves could not be
69 fully replicated. Hence, many of the existing formulations were derived and validated based on
70 incomplete insights and limited measurements of the complex hydrodynamic forces found
71 under breaking waves. This lack of process understanding resulting from a deficiency in

detailed measurements was reflected in the performance of the existing C_0 models, as presented in the work of Lim et al. (2020).

The present study follows on from the findings of Lim et al. (2020), which focused on evaluating the reference concentration, which in turn is used to determine the vertical concentration profile *C(s)*. Despite their importance in modelling morphodynamic changes, how well existing concentration profile *C(s)* models perform under field-scale breaking wave conditions is yet uncertain, as are the resulting implications of their performance on subsequent computations of transport rates and morphodynamic changes. The present study focuses specifically on the vertical distribution of suspended sand concentration. Here C_0 is prescribed using the validated L19 formulation (Lim et al., 2020) at a fixed near-bed reference level (100 * D_{50} above the bed), and attention is directed towards assessing and refining the profile models. In contrast to our previous work, which compared multiple reference concentration formulas, this study introduces a new approach to model the vertical SSC profile given a fixed C_0. The key novelty lies in improving the vertical concentration profile shape once C_0 is specified, rather than re-examining reference concentration formulas. Unlike Lim et al. (2020), which examined various C_0 models, here we focus only on *C(s)* profile shape. It is therefore the aim of the present study to quantitatively and qualitatively evaluate the performance of existing concentration profile *C(s)* formulae developed for breaking wave conditions against high-resolution (temporal and spatial) datasets collected under large-scale regular and irregular breaking waves in multiple cross-shore zones: the shoaling, breaking and inner surf zones.

The different formulae (new and existing) used to model *C(s)* under breaking wave conditions are detailed in *section 2*. Details regarding the different datasets used in the validation of the new and existing models are provided in *section 4*. The validation of model performance against each other, and against measured data, is provided with relevant discussions in *section 5*. Finally, *section 6* summarises the key conclusions of this paper.

2. Process-Based Framework for Suspended Sediment Profiles

The vertical distribution of suspended sediment concentration in coastal environments can be described using a balance between gravitational settling and turbulent mixing. Under steady conditions and neglecting horizontal advection, the vertical transport of suspended sediment can be expressed using the convection–diffusion equation:

$$w_s C + \varepsilon_s \frac{dC}{dz} = 0 \qquad (1)$$

where *C(s)* is the time-averaged vertical concentration profile (kg/m^3) – also known as suspended sand concentration (SSC) with respect to elevation above the bed (z); w_s is the grain settling velocity (m/s), ε_s is the sediment diffusivity coefficient.

This equation represents the balance between the downward settling of sediment particles and upward turbulent mixing. The resulting concentration profile therefore depends strongly on the assumed vertical structure of the sediment diffusivity $\varepsilon_s(z)$.

$$\varepsilon_s = \kappa u_* z$$

Where u_* is the bed shear velocity and κ is the von Kármán constant.

However, under breaking wave conditions, turbulence generation is not confined to the bed boundary layer. Recent numerical investigations of wave–structure interactions have also highlighted the limitations of conventional turbulence modelling approaches in resolving complex flow-sediment interactions, particularly under highly unsteady conditions such as wave breaking and overtopping (Jayaratne et al., 2025). These studies emphasise that turbulence generation can extend throughout the water column, supporting the need for enhanced representations of sediment diffusivity beyond classical near-bed assumptions. In the surf zone, strong turbulence is generated by wave breaking processes including plunging jets,

surface rollers, and large-scale vortices (Svendsen, 1984; Ogston & Sternberg, 2002). These processes can inject turbulence into the mid and upper regions of the water column, resulting in vertical mixing structures that differ significantly from classical boundary layer assumptions.

As a result, sediment diffusivity profiles under breaking waves may deviate substantially from the linear distribution assumed in the Rouse formulation. Several alternative concentration profile models have therefore been developed, each representing different assumptions regarding turbulence structure and sediment mixing processes.

Table 1 summarizes the conceptual differences between the concentration profile models evaluated in this study, highlighting the underlying assumptions regarding sediment diffusivity and turbulence generation mechanisms.

Table 1. Conceptual basis of concentration profile models

Model	Diffusivity assumption	Turbulence source
Rouse (1939)	$\varepsilon = \kappa u_* z$	Bed-generated turbulence
SR93	ε linked to wave energy dissipation	Breaking-induced turbulence
LK01	Constant ε	Fully mixed water column
JS07	Includes wave-current interaction	Combined shear + wave motion
W12	Includes orbital velocity effects	Wave boundary layer

This process-based framework provides a consistent basis for comparing different concentration profile formulations and evaluating their applicability under breaking wave

conditions. In the present study, these models are assessed against large-scale laboratory datasets to examine their ability to reproduce observed suspended sediment concentration profiles across different cross-shore regions.

3. Overview of C(s) Models

The vertical distribution of SSC has been expressed using several profile forms:

- Rouse profile (Eq. 2): derived from a balance between gravitational settling and upward turbulent mixing. It predicts a power-law distribution in which concentration decreases with height, controlled by the Rouse number.
- Power-law profiles (Eq. 6): empirical formulations (e.g., SR93; JS07) where concentration decays with elevation following an exponent that can be tuned to experimental data. These profiles often provide flexibility but lack a clear physical interpretation.
- Exponential profiles (Eq. 11): assume concentration decreases exponentially with height above the bed, consistent with turbulence intensity decay. This form is less widely applied but provides a simple representation of rapid vertical decay.

The choice of profile form strongly influences the implied reference concentration at a chosen elevation and therefore must be handled consistently when comparing models.

Rouse (1939) – R39

One of the most widely used concentration profile formulae are either variations of, or based on the simple power function referred to as the 'Rouse profile' equation, which can be expressed as (e.g. van Rijn, 2007):

$$C(z) = C_0 \left\{ \left[\frac{(d-z)}{z} \right] \left[\frac{a}{(d-a)} \right] \right\}^M \qquad (2)$$

where d is the local water depth (m), z is the distance above bed (m), a is the reference level (m), M is the dimensionless mixing parameter, based on the well-known Rouse number:

$$M = \frac{w_s}{\kappa u_*} \qquad (3)$$

where κ is the von Karmen constant (=0.4) and u_* is the bed-shear velocity (m/s). Thus, M is the classic Rouse number (dimensionless mixing parameter).

Shibayama & Rattanapitikon (1993) – SR93

For non-breaking conditions, Shibayama & Rattanapitikon (1993), henceforth abbreviated to SR93) proposed an exponential formula derived from the steady diffusion equation to predict the time-averaged concentration profile. They predicted however that an exponential concentration profile or uniform value of the diffusion coefficient would not be suitable for breaking wave conditions. Based on experimental data and the assumption that the diffusion coefficient is proportional to the eddy viscosity of flow, Shibayama & Rattanapitikon (1993) adopted the concept of Okayasu (1989) who suggested that a linear distribution of the eddy viscosity (ε_v) was proportionate to the rate of wave energy dissipation due to wave breaking (D_B).

Larson & Kraus (2001) – LK01

Larson & Kraus (2001, abbreviated to LK01) assumed that, under breaking waves, the time-averaged turbulence intensity was homogenous throughout the water column and that the vertical distribution of suspended sediment concentration ($C(s)$) was proportional to $\exp[-(w_s/\varepsilon_s)z]$, where the ε_s is the sediment-mixing or diffusion coefficient. It should be noted that LK01 also implies an exponential concentration profile.

180 **Jayaratne & Shibayama (2007) – JS07**

181 Jayaratne & Shibayama (2007, abbreviated to JS07) accounted for local TKE by including the
182 shear velocity under the wave-current co-existent field (u_{*wc}), and included the breaking energy
183 dissipation model of Rattanapitikon & Shibayama (1998) to represent the external breaking-
184 generated TKE. Though elements of turbulent velocities induced by both waves (e.g. orbital
185 velocity) and currents (e.g. shear velocity) were incorporated into the formulation, the high
186 flow velocities induced by breaking-generated vortices were not explicitly accounted for in the
187 JS07 model.

188 **Wang et al. (2012) – W12**

189 Having carried out some comprehensive analysis of the performance of the LK01 concentration
190 profile model, and that of Nielsen (1986), Wang et al. (2012) proposed that the existing LK01
191 model could be improved by incorporating the effects of wave orbital motion and bottom shear
192 stress (as done by Nielsen, 1986 - henceforth referred to as N86) into a combined formula. This
193 was because each of the existing models (LK01 and N86) incorporated different processes that
194 induced sediment entrainment and vertical mixing. The LK01 model assumed that the wave
195 breaking-induced turbulence and associated wave-energy dissipation was the sole cause of
196 sediment suspension and the primary factor influencing the suspension patterns (Wang et al.,
197 2012). Wang et al. (2012) argued that although breaking-induced TKE is the dominant cause
198 of sediment pickup and mixing in the surf zone, effects of near-bottom shear and wave orbital
199 velocities do still contribute to the concentration profile and therefore should be incorporated
200 into *C(s)* models for breaking wave conditions.

201 **3.1 Modified *C(s)* Model**

202 It should be noted that the modified *C(s)* model described herein was developed after the
203 validation of existing *C(s)* models, which is presented in sections 5.2-5.6. The details of the

model development are however presented here, so that all information regarding model development/conditions can be seen in a single section.

In section 5, existing *C(s)* models such as SR93 and JS07, which use the power function equation, are found to over-predict concentration in the upper water column (where $z/d > 0.2$), even when agreement is good in the lower water column. This is because the magnitude of the computed dimensionless mixing parameter (M) is too small (generally < 0.5), causing the resulting concentration profile curves to be steep and quasi-uniform/linear on the log-scale (i.e. almost perpendicular to the x-axis).

To provide a more physically meaningful interpretation, the coefficient B can be related to the turbulent Schmidt number, which represents the ratio between the eddy viscosity of the flow and the sediment diffusivity:

$$S_c = \frac{\nu_t}{\epsilon_s}$$

or equivalently:

$$\beta = \frac{\varepsilon_s}{\nu_t}$$

In classical sediment transport formulations, the Schmidt number is often assumed to be of order unity, implying that the turbulent mixing of sediment and momentum occur at similar rates. However, under breaking wave conditions, this assumption may not hold.

Breaking waves generate strong turbulence not only near the bed but also in the mid and upper regions of the water column due to plunging jets, surface rollers, and large-scale vortical structures (Svendsen, 1984; Ogston & Sternberg, 2002). These processes enhance vertical sediment mixing beyond what is predicted by bed-generated turbulence alone.

As a result, the effective sediment diffusivity may differ significantly from the eddy viscosity, leading to Schmidt numbers greater than unity. Previous experimental studies have reported Schmidt numbers ranging between approximately 1 and 5 under energetic wave and surf zone conditions (van Rijn, 2007; Thorne et al., 2009).

Within this context, the coefficient *B* introduced in the present study can be interpreted as an effective scaling factor accounting for enhanced turbulent mixing under breaking waves. The calibrated value of *B*=3.3 falls within the range of Schmidt numbers reported in the literature, suggesting that the modified formulation reflects physically realistic mixing conditions rather than purely empirical tuning.

This interpretation provides a physical basis for the modification of the mixing parameter and supports its applicability across different breaking wave conditions.

The implementation of a constant *B* is applicable to concentration profile formulations based on power-law relationships. It was tested on both the SR93 and JS07 models, but as described in section 5.7., of the two formulae, the JS07 model produces marginally higher values of *C(s)* in all cross-shore zones. As the initial issue was that the SR93 and JS07 models were overpredicting *C(s)* in the upper water column, it was logical to implement the *B* constant into the formula that produced lower values of *C(s)*. Hence, the *B* constant was added to the SR93 mixing parameter, forming a modified SR93 profile (denoted as the 'L19 *C(s)*', where L19 refers to the Lim et al. 2020 model name). The same power function *C(s)* formula is used, but an alternative mixing parameter *M* is used as shown below:

$$M = B\left(\frac{w_s}{\varepsilon_b}\right) \qquad (4)$$

Where B is a dimensionless coefficient representing the effective turbulent Schmidt number, accounting for the ratio between sediment diffusivity and eddy viscosity under breaking wave

conditions. Details of the implementation and calibration of the constant B are provided in section 5.7 under the 'Proposed Modified $C(s)$ Model' sub-section. Further details on the constituent parameters and key assumptions made for the original SR93 $C(s)$ formulae are provided in section 3 and are therefore not repeated here. This modification is therefore consistent with a process-based interpretation of sediment diffusivity under breaking waves.

3.2 Reference Concentration Model (C_0)

A considerable number of studies have endeavoured to model the SSC at the near-bottom reference level, i.e. the reference concentration (C_0). Some have related the reference concentration to the bed shear stress or bed shear velocity, or the dimensionless bed shear stress - i.e. Shields parameter (e.g. Van Rijn, 1984; 1993; 2007; Shibayama & Rattanapitikon 1993; Camenen & Larson, 2008), others to the local wave height, water depth or relative wave height (e.g. Mocke & Smith, 1992) or the wave height at the breaking point (e.g. Jayaratne & Shibayama, 2007), energy dissipation of the surface roller (e.g. Smith & Mocke, 1993; Spielmann et al., 2004) and inclusion of near-bed TKE to increase bed shear stress (e.g. Hsu & Liu, 2004; Okayasu et al., 2010; Van der Zanden et al. 2017c).

As mentioned in earlier sections of this paper, Lim et al. (2020) carried out an extensive evaluation of existing reference concentration models, identifying key limitations and suggesting solutions to overcome them. The most common limitations found in the existing C_0 models were separated into two categories: 1) inapplicability of the model to multiple cross-shore zones (e.g. to shoaling, breaking and inner surf zones), and 2) inability to account for the strong localised increases in suspended sand concentration found in the breaking zone (Lim, 2021). Lim et al. (2020) developed a new practical reference concentration model for breaking

wave conditions to address these limitations, incorporating a novel relationship observed between the local water depth (d) and the cross-shore distribution of C_0:

$$C_0 \propto 1/d$$

Under both regular and irregular prototype-scale breaking wave conditions, with and without the presence of a breaker bar, the inverse of the local water depth was found to correlate strongly with the cross-shore distribution of C_0, indicating that as the depth decreased (from the shoaling to the breaking zone) the corresponding concentration increased. This trend was observed to be applicable in the shoaling and breaking zones, but not the inner surf zone. This relationship between C_0 and d was utilised to empirically account for the increases in SSC observed between the shoaling and breaking zones. Additionally, key parameters representing the average grain diameter, gravitational (settling) forces on sand grains, wave energy dissipation and wave climate were incorporated to model the reference concentration in kg/m^3 at a reference level of $100\times D_{50}$:

$$C_0 = (\gamma D_*)^{-0.695} \cdot g\left[\left(\frac{\Omega}{D_r}\right)^{1.9}\right] \cdot \frac{T}{d} \qquad (5)$$

where

γ = dimensionless constant = 0.0464

Ω = dimensionless constant related to cross-shore region

- For erosive wave cases:

Ω = 7.5-15.0 for shoaling and breaking regions

Ω = 1.0-3.0 for inner surf zone

- For accretive wave cases:

294 Ω = 1.5 for breaking and shoaling zones

295 Ω = 0.6 for inner surf zone

296 $$D_* = D_{50}\left[\frac{(s-1)g}{\nu^2}\right]^{\frac{1}{3}} \quad (6)$$

297 where,

298 D_* is the dimensionless grain diameter (van Rijn, 2007)

299 D_{50} = average grain diameter (m)

300 s = specific gravity (-)

301 υ = kinematic viscosity (m^2/s)

302

303 $$D_r = 2\beta g\frac{E_r}{c} \quad (7)$$

304 where

305 D_r = roller dissipation rate (kg/s^3)

306 β = coefficient related to the wave steepness = 0.1

307 c = wave celerity (m/s) = $\sqrt{(g \cdot d)}$

308

309 $$E_r = \rho_w\frac{Ac^2}{2L} \quad (8)$$

310 where

311 E_r = the roller energy (kg/s^2)

312 ρ_w = density of water (kg/m^3)

313 A = roller area estimated empirically as $0.9H^2$ by Svendsen (1984) (m^2)

314 L = wavelength estimated using linear wave theory (m)

315

316 Full details of the modelling philosophy, development and calibration can be found in Lim at
317 al. (2021).

318 **4. Datasets**

319 Only key information required for the computation of *C(s)* and interpretation of findings are
320 provided in this paper. For more details on the experiment conditions, profile evolution, test
321 runs, instrumentation, etc. readers are directed to Lim et al. (2020).

322 **4.1. LIP Experiments – Roelvink & Reniers (1995)**

323 The Large Installation Plan (LIP) experiments were carried out in the Delta Flume (225×5×7
324 m- L×W×D) at Delft Hydraulics. Note: the LIP experiments consisted of two different types
325 of irregular breaking waves: 1) erosive conditions and 2) accretive conditions. Both were run
326 using the same test conditions except for the wave period and target significant wave height.
327 For the erosive (accretive) case, the target peak wave period was 5 s (8 s), and the target
328 significant wave height was 1.4 m (0.6 m). More details are available in Roelvink and Reniers
329 (1995).

330 **4.2. CROSSTEX Experiments – Yoon & Cox (2010)**

331 The CROSSTEX dataset was measured in the O H Hinsdale Laboratory of Oregon State
332 University, USA. Note: similar to the LIP dataset, the CROSSTEX experiments consisted of
333 two different types of irregular breaking waves: 1) erosive conditions and 2) accretive
334 conditions. Both were run using the same conditions except for the wave period and target
335 significant wave height. For the erosive (accretive) case, the target peak wave period was 4 s
336 (7 s) and the target significant wave height was 0.6 m (0.4 m).

For the erosive case and accretive case, 11 runs (E1-E11) and 9 runs (A1-A9) were carried out respectively. Both spilling and plunging breakers were observed in the erosive and accretive cases, but spilling breakers were prevalent in the erosive case and plunging breakers prevalent in the accretive case. Each experimental run lasted approximately 15 minutes, with only a few runs in the accretive case running for 45 minutes. The total run time for the erosive and accretive cases were 180 and 300 minutes respectively. More details are available in Yoon and Cox (2010).

4.3. SandT-Pro Experiments – Ribberink et al. (2014)

The Sand Transport Process measurements under Breaking and Irregular Waves (SandT-Pro) dataset was measured in the Canal d'Investigació i Experimentació Marítima (CIEM) Flume in the Polytechnic University of Catalunya (UPC), Barcelona. Two different experiments were run: Regular Breaking 1 (RB1) and Regular Breaking 2 (RB2). Only the RB1 experiments are covered in this paper, and henceforth all reference to the SandT-Pro dataset is referring to the RB1 experiments. A mobile bed (with offshore bed slope was 1:10) was made in the flume consisting of sand with an average grain diameter D_{50} = 0.246 mm. More details are available in Ribberink et al. (2014).

4.4. SINBAD Experiments – Van der Zanden et al. (2016)

Like the SandT-Pro dataset, the SINBAD dataset (Van der Zanden et al., 2016) was also measured in the CIEM Flume in the Polytechnic University of Catalunya (UPC), Barcelona. A mobile bed (with offshore bed slope of 1:10) was made in the flume consisting of sand with an average grain diameter D_{50} = 0.246 mm (D_{10} = 0.15 mm and D_{90} = 0.37 mm). More details are available in Van der Zanden et al. (2016).

5. Validation & Discussion

The measured concentration profiles presented in this section consistently exhibit concave shapes, characterised by elevated near-bed concentrations and reduced values towards the water surface. From a process-based perspective, such profiles indicate enhanced turbulent mixing extending beyond the near-bed region.

Under breaking wave conditions, turbulence generated by plunging jets, surface rollers, and large-scale vortices can inject energy into the mid and upper water column. This leads to sediment diffusivity profiles that differ significantly from classical bed-generated turbulence assumptions.

The improved performance of the modified model can therefore be interpreted as a consequence of incorporating enhanced effective sediment diffusivity, represented through the parameter B, which accounts for increased turbulent mixing under breaking waves.

The concentration profile $C(s)$ simply refers to the vertical distribution (as a function of elevation above bed, z) of the suspended sand concentration. In order to focus only on the differences in performance resulting from the variations in concentration profile $C(s)$ formulations used, all analysis carried out in this section was done using the same reference concentration C_0 model. The reference concentration (C_0) is one of the major parameters in computing the $C(s)$, and therefore it is essential that C_0 is accurately modelled in order to obtain accurate computed concentration profiles. As the C_0 formula of L19 (Eq. 5, section 3.2) showed very good agreement in the validation presented in the work of Lim et al. (2020), it is used to compute C_0 for all cases shown herein, and the various concentration profile formulae are used to compute $C(s)$.

The Rouse, power-law, and exponential profiles each define the reference concentration at different elevations above the bed (za), leading to different implied C_0 values even under

identical forcing conditions. As a result, earlier comparisons may have conflated differences in profile shape with differences in C_0 definition. In the present work, this issue is addressed by adopting a consistent C_0 (from L19) across all cases and evaluating only the vertical distribution prescribed by each profile form. We note that this approach fixes the near-bed concentration for all models (using L19) rather than fitting each profile's own optimal C_0, this controlled comparison highlights differences in profile shape alone. While using measured C_a at a known reference height for each model would be ideal, such data were limited, so a common C_0 was chosen for consistency.

In all plots presented in this paper, the left column of plots shows *C(s)* in the shoaling zone (pre-breaking), the centre column of plots shows *C(s)* in the breaking zone (around the plunging/spilling point), and the right column of plots shows *C(s)* in the inner surf zone (post-plunging). The plots in this section follow the same design, showing the measured against computed concentration profiles. The measured profile is named after the dataset used in each plot, and the computed profile is named after the formulae used to compute it (e.g. concentration profile computed using the formulae of Shibayama and Rattanapitikon, 1993, is referred to as 'SR93' in plots). The *y*-axis has been normalised to allow for inter-comparison of trends between multiple datasets and transport models.

5.1. Measured Concentration Profiles

The different measured concentration profiles shown in Fig. 1 indicate a similar pattern over the cross-shore regions. Generally, prior to plunging (left column of plots: shoaling zone), concentration levels are relatively low, in the order of 10^{-1} kg/m^3. The magnitude of sediment concentration declines substantially from the breaking to the inner surf zone, where in most cases the measured SSC is less than 1 kg/m^3. Even still, the concentration profiles are quite

steep (almost perpendicular to x-axis), indicating that concentration levels are quasi-uniform throughout the water column.

Under spilling breakers (erosive cases), the measured concentration profile changes very little between shoaling, breaking and inner surf zones, with the shape of the profile of concentration remaining relatively constant throughout the whole water column (see Fig. 1a-c, g-i). Under spilling/weakly-plunging waves (e.g. Fig. 1b, e, h), the measured concentration profile indicates a quasi-uniform level of concentration (i.e. almost perpendicular to x-axis), but under strong plunging breakers (e.g. Fig. 1k, n, q) the near-bed concentration is seen to rise drastically. Near the bottom, concentration reached almost 10 kg/m^3 under strong plunging waves. At this point, the measured profile increases exponentially near the bed (z/d < 0.2) but SSC in the upper water column (outer region) increases at a slower rate (i.e. the curve is more gradual).

5.2. Rouse (1939) – R39

Unlike other *C(s)* models covered in this paper, the performance of the R39 model seems to be unaffected by the cross-shore region, or even the breaker type, but highly sensitive to the elevation above bed (z) at which the measurement is taken. Predicted *C(s)* is generally in the correct order of magnitude in the near-bed region (z/d < 0.1), but there are very large discrepancies in the upper water column. This is the case, even when there is good agreement in the near-bed region (e.g. Fig. 1a, c, p, q), with discrepancies getting increasingly larger as z approaches the surface (i.e. where $z = d$). In the upper water column, the magnitude of computed *C(s)* is frequently seen to be smaller than measured *C(s)* by two orders of magnitude and in some cases even more. Assuming that all computed concentration values lower than 0.01 kg/m^3 in Fig. 1 are negligible (=0), the guidelines provided by van Rijn (2007), which classify M < 0.7 as indicating near-bed confinement, for the Rouse number (M) can be compared against modelled results.

431 Most of the plots shown in Fig. 1 indicate that the dimensionless Rouse Number (mixing
432 parameter) has a value between 1-3, with a few cases being marginally larger or smaller. Figs.
433 6a-b for example have values of M = 1.57 and 1.70, respectively. Thus, they fall between the
434 second and third categories from the van Rijn (2007) guidelines, indicating that they should
435 have suspended sediment going up to a level between the water surface and the middle of the
436 water depth.

437 Evaluating the performance of the R39 model quantitatively, the RMSE values shown in Tables
438 12 and 13 at the end of section 4.7. indicate that the discrepancies between computed and
439 measured concentration seem to be marginal in terms of magnitude. This is seen to be the case
440 even in plots where performance is clearly poor from a qualitative standpoint. For example, in
441 Figs. 6a-c, despite the large disparity between measured and computed points seen in the upper
442 water column, the RMSE ranges between 0.29-1.89 kg/m^3, which is relatively small.

443

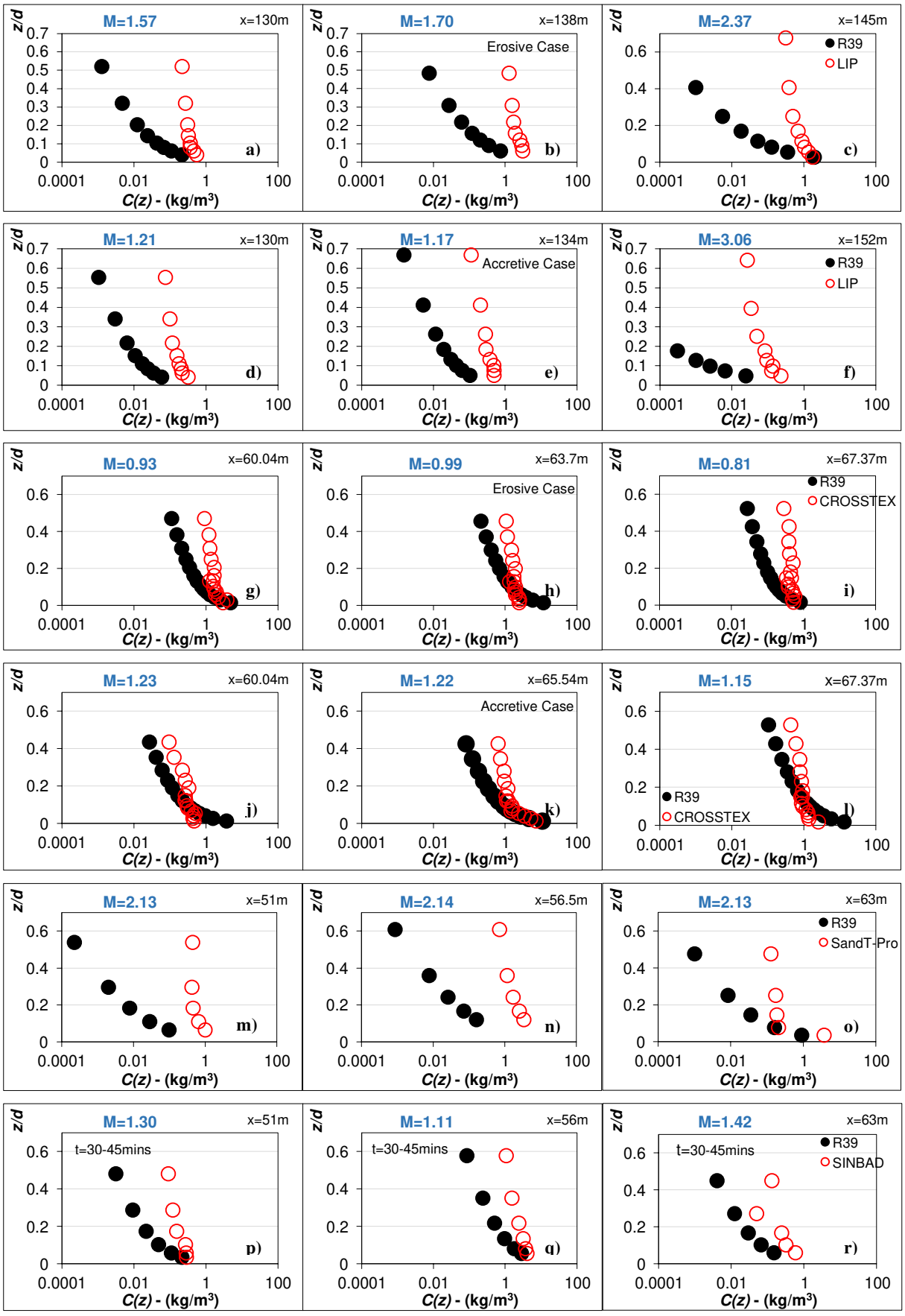


Figure 1 - Concentration profile (C(z)) of Measured (red circles) vs. computed (Rouse (1939)-R39, black circles) concentration.

444

5.3. Shibayama & Rattanapitikon (1993) – SR93

In the shoaling zone, SR93 largely shows reasonable-good agreement with measured data throughout the whole water column (e.g. see Fig. 2a, d, g). This is also the case in the breaking zone, under spilling wave conditions and even under some weaker plunging waves (e.g. Fig. 2b, e), indicating that the *C(s)* formulae of SR93 are fairly adept in replicating the concentration profile under breaking wave conditions. SR93 however does sometimes over-predict concentration in the upper water column ($z/d > 0.2$), despite agreement in the near-bed region being good. This indicates that the discrepancy between measured and computed profiles is not resulting from the reference concentration model, but the concentration profile model of SR93.

Throughout Fig. 2, the SR93 concentration profile is quite steep (almost perpendicular to the x-axis, particularly in the outer region, $z/d > 0.1$) indicating a quasi-uniform distribution of SSC in the whole water column. This steep curve is reasonably suitable for the shoaling zone where there is a constant, relatively low level of measured SSC in the whole water column. Even in the breaking zone, under spilling/irregular plunging breakers, the SR93 model is seen to perform reasonably well. Under the regular plunging breakers however discrepancies are found in the upper water column, indicating overprediction.

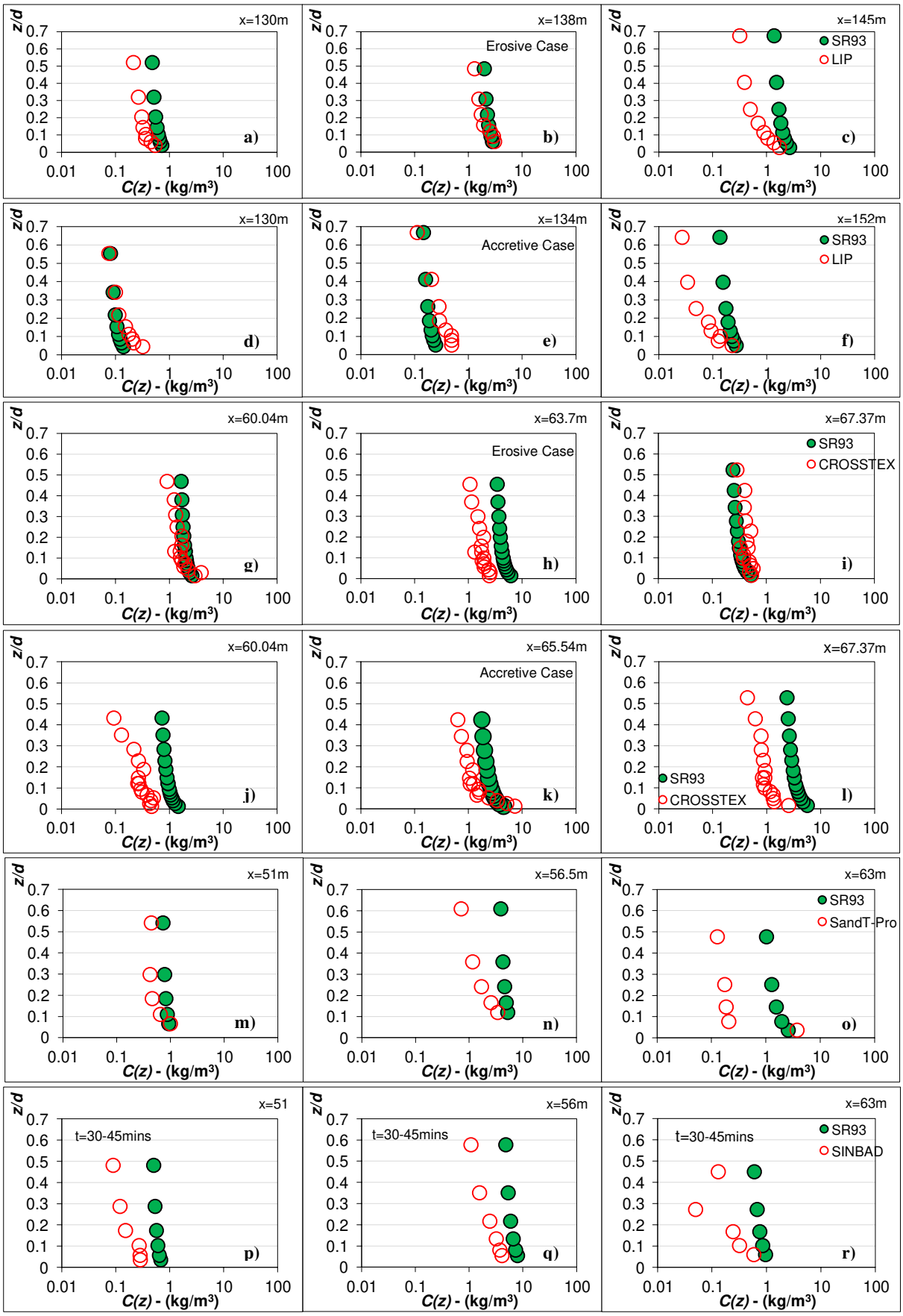


Figure 2 - Concentration profile (C(z)) of Measured (red circles) vs. computed (Shibayama & Rattanapitikon (1993)-SR93, green circles) concentration.

461

462 **5.4. Larson & Kraus (2001) – LK01**

463 Wang et al. (2012) reported that for the spilling breaker case, the value of k_d = 0.03
464 (recommended by Larson & Kraus, 2001) resulted in concentration profiles that were too steep
465 at most cross-shore locations, and that a value of k_d = 0.01 produced more gradual profiles that
466 better fit the measured values. The only exceptions were reported at the secondary breaker line,
467 where k_d = 0.03 produced a closer fit to measured concentration. For the plunging breaker case,
468 Wang et al. (2012) reported that k_d = 0.01 produced better agreement in the mid-surf zone but
469 k_d = 0.03 produced better agreement near the plunging point and near the secondary breaker
470 line. These findings differ slightly from those of Wang et al. (2012), which may be attributed
471 to scale effects. Our large-scale experiments exhibited stronger turbulent mixing and higher
472 SSC throughout the water column than the smaller-scale LSTF experiments. The greater
473 turbulence in our tests (rather than sediment grain size differences) can explain why a higher
474 diffusion coefficient (k_d = 0.03) consistently fit our data better.

475 The measured concentration profiles in this study were generally steeper than those from the
476 LSTF dataset (c.f. Wang et al., 2002; Wang et al., 2012), in both the spilling and plunging cases.
477 This indicates that there were high levels of SSC not only near the bed, but in the upper water
478 column also. Assuming that the high concentration in the upper water column indicates
479 enhanced vertical sediment mixing, this suggests that vertical sediment mixing was more
480 prominent in the datasets used in this paper than in the LSTF dataset (Fig. 3). Comparing the
481 wave conditions from the LSTF dataset against those used in the present paper indicate that the
482 wave heights, wavelength, wave period and water depth were considerably smaller in the LSTF
483 experiments (a brief summary of the LSTF test conditions can be found in Table 2).

484 Furthermore, the average grain diameter from the LSTF dataset was 0.15 mm, which is much
485 smaller (finer) than that used in this paper, where D_{50} ranged between 0.22-0.25 mm. The grain

settling velocity of 0.018 m/s for LSTF was also much lower than those presented in section 3 which ranged between 0.030-0.034 m/s. Finer sediment generally takes longer to settle, hence the lower settling velocity, and also less resistance to entraining forces. One would therefore predict higher levels of SSC under the LSTF experiments, but this is contrary to what is seen in the data. Therefore, it is suggested that the difference was not due to the sand characteristics, but due to variations in turbulence structure observed under the relatively smaller-scale LSTF experiments.

Table 2 - Summary of LSTF dataset (c.f. Wang et al. 2002)

Mobile sand bed	Yes: D_{50} = 0.15 mm
Computed settling velocity	0.018 m/s
Regular or Irregular waves	Irregular (erosive and accretive)
Breaker types	Spilling and plunging
Offshore wave height (H_0)	Spilling case: 0.25 m, Plunging case: 0.23 m
Offshore wave period (T)	Erosive case: 1.5 s, Plunging case: 3.0 s

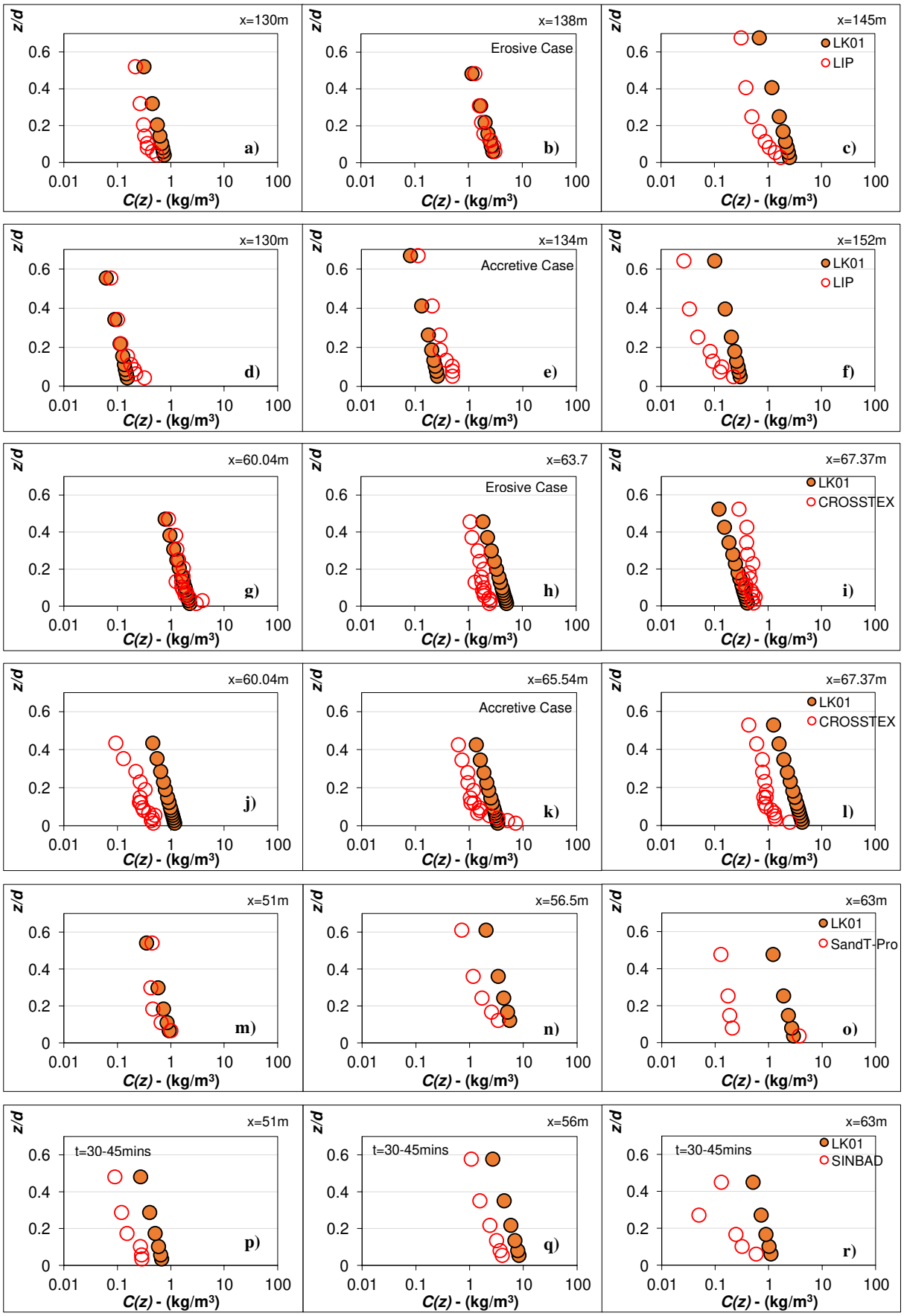


Figure 3 - Concentration profile ($C(z)$) of Measured (red circles) vs. computed (Larson & Kraus (2001)-LK01, orange circles) concentration.

5.5. Jayaratne & Shibayama (2007) – JS07

The performance of the JS07 model is almost identical to that of the SR93 model – the shape of the profile is almost the same in all three cross-shore zones, with the computed values of JS07 being marginally greater than those of SR93. The two models were essentially modelled in the same way, with both using the same power function *C(s)* model. The main differences between the two formulations however were the minor differences in values used for constants k_1 and k_2 in the computation of diffusion coefficient (ε_b), the use of the shear velocity under wave-current coexistent field instead of the shear velocity parameter (refer to sections 2.1.2. and 2.1.4. to see differences between these parameters), and the different formulations implemented for computing the rate of wave energy dissipation (D_B). Of these, the difference in D_B formulation is the most major, with SR93 using the formulae of Thornton & Guza (1983), and JS07 using the formulae of Rattanapitikon and Shibayama (1998). Despite these noticeable differences however, the effects on the resulting concentration profiles could be considered negligible.

Just like the performance of the SR93 *C(s)* model indicated over-prediction to varying extents in all three cross-shore zones, the same is seen of the JS07 *C(s)* formulae, with relatively large over-prediction found in the upper water column (e.g. Fig. 24 k, n, q, where RMSE ranges between 1.5-4.71 kg/m^3). Discrepancies in the upper water column between JS07 and measured concentration were as large as 5.2 kg/m^3, which is almost 5 times larger than the corresponding measured concentration at that cross-shore location. This large disparity in the upper water column is largely related to the mixing parameter (M) which ranges between 0.1-0.2. Though the mixing parameter of JS07 is formulated differently to the Rouse profile, it can still be compared against the guidelines provided by van Rijn (2007) mentioned in section 4.2. According to the guidelines of van Rijn, $M = 0.1$ results in suspended sediment being almost

520 uniformly distributed over the whole water depth. This is consistent with what can be observed
521 in Fig. 4, in which JS07 predicts quasi-uniform concentration in the whole water column in all
522 tested cases, regardless of cross-shore region. Therefore, it does not well-represent the
523 commonly seen concave shape of the measured profiles, which indicate higher concentration
524 near the bed and gradually lower concentration towards the surface. It is suggested that the
525 introduction of a new constant or parameter to increase the magnitude of M will result in a
526 more gradual and parabolic concentration profile that more closely mirrors the measured
527 profile. This is further discussed under the "Proposed Modified $C(s)$ Model" subsection later
528 in this paper.

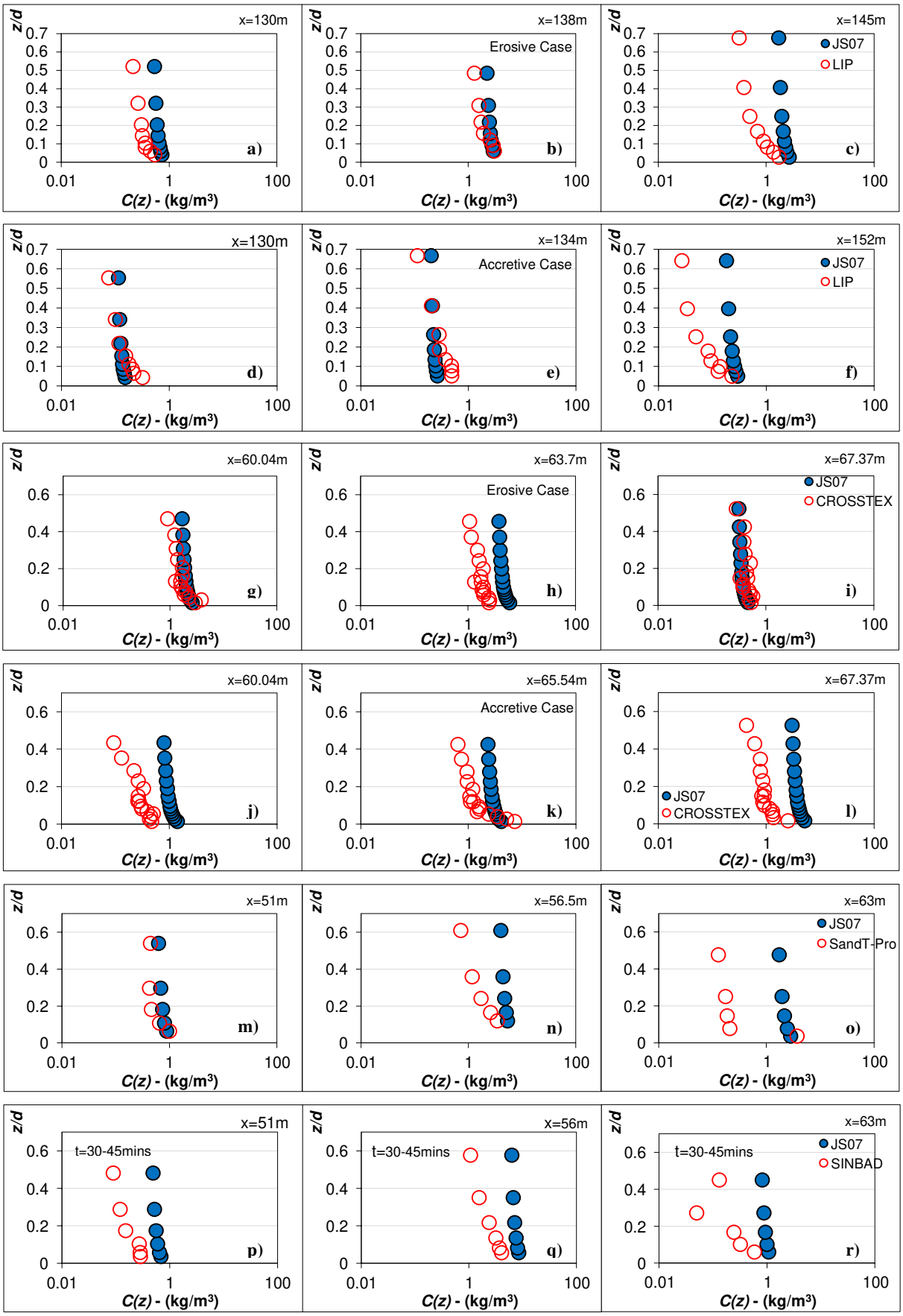


Figure 4 - Concentration profile ($C(z)$) of Measured (red circles) vs. computed (Jayaratne & Shibayama (2007)-JS07, blue circles) concentration.

529

530 Plots a-c show LIP erosive, and d-f show LIP accretive cases respectively; plots g-i show
531 CROSSTEX erosive and j-l show CROSSTEX accretive cases respectively; plots m-o show
532 SandT-Pro and plots p-r are SINBAD. Each row of plots shows three different cross-shore
533 locations: before the breaking point (left plots), at the breaking or plunging point (central plots)
534 and onshore of the breaking point (right plots).

535

536 **5.6. Wang et al. (2012) – W12**

537 As mentioned in section 2.1.5., the Larson-Kraus-Nielsen model is referred to here as Wang et
538 al. (2012) or W12 for short, as Wang et al. (2012) integrated the Larson-Kraus (LK01) model
539 with the model of Nielsen to produce an improved *C(s)* model for breaking wave conditions.
540 Despite the implementation of the intensity and length scale of wave orbital motion into the
541 original formula of LK01, the resulting differences in performance appear to be quite small in
542 Fig. 5.

543 Unlike the SR93 and JS07 concentration profile models, which produce (mildly) parabolic
544 profiles, the models of LK01 and W12 produce profiles which appear to be linear on the log-
545 scale. As such, the parabolic shape of the measured profiles is often not well-mirrored, with
546 computed profiles appearing more like a 'line of best-fit' through the measured concentration
547 points (e.g. Fig. 5k). This means that the performance of these formulae is relatively more
548 dependent on the accurate prediction of the reference concentration, as the reference
549 concentration practically serves as the starting point on the best-fit line. Regardless however
550 the model of W12 generally performs well, with relatively good agreement with measured data
551 in all three zones, throughout the whole water column.

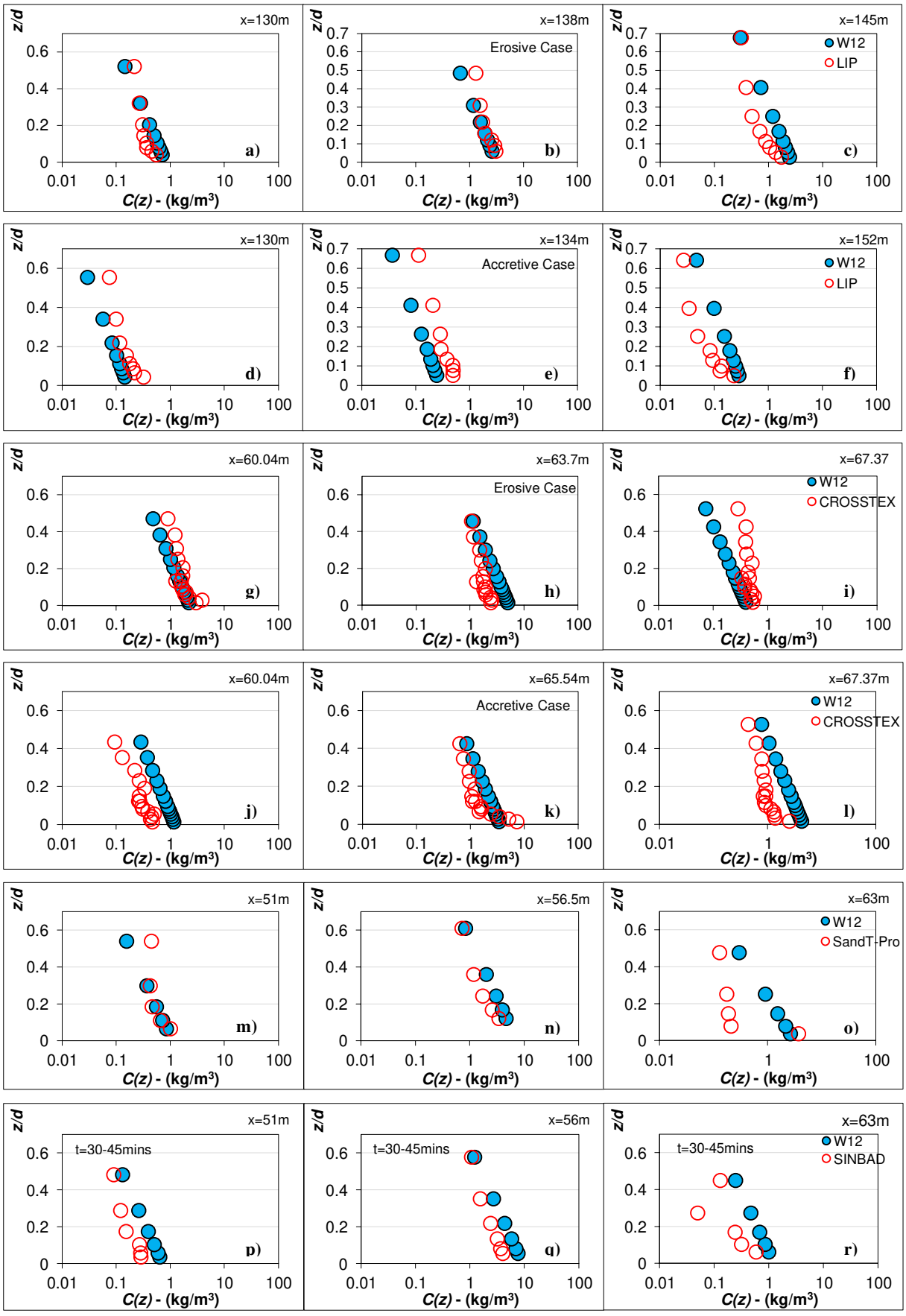


Figure 5 - Concentration profile ($C(z)$) of Measured (red circles) vs. computed (Wang et al. (2012)-W12, light blue circles) concentration.

552

553 ### 5.7. Proposed Modified *C(s)* Model

554 As the L19 *C(s)* model is a modification of the SR93 formula (as described in section 2.2.), a
555 new value for the constant *B* is applied and results are compared herein against the original
556 plots from SR93. Agreement between measured and computed *C(s)* shown in Fig. 2f (from the
557 subsection "Shibayama & Rattanapitikon, 1993"; where essentially *B* = 1 (unit less)) is
558 improved significantly by multiplying the mixing parameter (*M*) by a constant *B* = 3.3. This
559 value of *B* was tuned to minimise RSME across cases and was determined based on some
560 empirical analysis which was carried out on a couple of test cases. The test plots from the
561 calibration analysis are shown in Fig. 6.

562

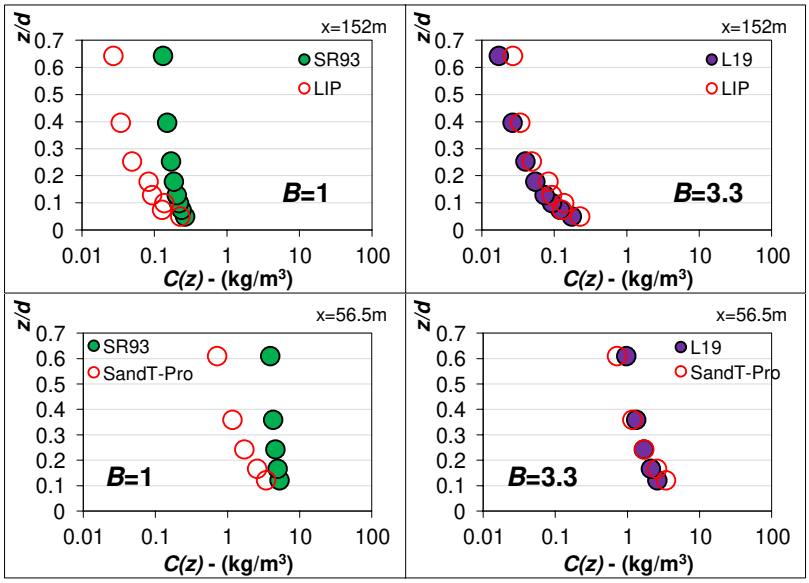


Figure 6 - Concentration profile (*C(z)*) of Measured vs. computed (SR93, green circles on left plots) vs. computed (L19, purple circles on right plots) concentration.

563

564 Left plots show original SR93 plots: top left plot from Fig. 2f (i.e. where constant *B* = 1) and
565 bottom left plot from Fig. 2n. Right plots show the new L19 concentration profiles with
566 constant *B* = 3.3, top right plot shows Fig. 2f with new *B* value and bottom right plot shows
567 Fig. 2n with new *B* value.

568 Figure 6 shows that the simple incorporation of a constant (>1) changes the shape of the
569 resulting concentration profiles and also deals with the overprediction found throughout the
570 whole water column. Based on the improved predictions of the concentration profile observed
571 in Fig. 6, the constant value of $B = 3.3$ was applied to all plots. The new profiles (with $B = 3.3$)
572 are shown in Figure 7.

573 Upon comparison between Figs. 2 and 7, it can clearly be seen that the incorporation of the
574 dimensionless constant $B = 3.3$ has resulted in improved agreement between measured and
575 computed $C(s)$ in most plots, particularly in the breaking and inner surf zones (centre and right
576 columns of Fig. 7 respectively). Just as it was seen in Fig. 6, the over-prediction seen in every
577 plot of Fig. 2 (original SR93 formula) has been resolved, and the shape of the concentration
578 profile has been made more parabolic, better mirroring the measured profile. The improved
579 performance of the modified (L19) $C(s)$ model can also be seen in the RMSE values presented
580 in Table 2, where L19 produces substantially smaller RMSE than the SR93 model in 14/18
581 cases over all 4 datasets (RMSE for SR93 ranged between 0.08-3.62 kg/m^3 with an average of
582 1.04 kg/m^3; RMSE for L19 ranged between 0.03-2.13 kg/m^3 with an average of 0.56 kg/m^3).

583 As the modification of the mixing parameter was aimed at reducing the magnitude of the
584 suspended sand concentration overall (as well as modifying the profile shape), there are now a
585 couple of instances of under prediction seen in Fig. 7d and e. Considering however that these
586 discrepancies are not very large (within in the same order of magnitude, with RMSE = 0.13
587 and 0.27 kg/m^3 for Figs 7d and e respectively), and the vast improvements seen in the majority
588 of the plots in Fig. 7, it would seem that the implementation of the constant B was effective in
589 improving the concentration profile formulae of SR93. As the JS07 concentration profile model
590 uses the same formula as SR93 to compute the concentration profile (Eq. 6), it suffers the same
591 limitations as the original SR93 formula. Analysis (not shown) indicate that the implementation
592 of the constant B can be used as a solution for the JS07 formula also.

593

594 **Table 3** - RMSE for individual test cases of *C(s)* models (kg/m^3).

		R39	SR93	LK01	JS07	W12	L19
SINBAD	Shoaling	**0.14**	0.39	0.32	0.38	0.24	0.19
	Breaking	1.64	3.62	3.47	4.71	2.47	**0.61**
	Inner surf	0.25	0.51	0.60	0.69	0.41	**0.06**
SandT-Pro	Shoaling	0.58	0.28	0.20	0.20	0.23	**0.16**
	Breaking	1.90	2.78	2.03	2.88	1.02	**0.40**
	Inner surf	1.16	1.22	1.63	1.71	1.11	**0.89**
CROSSTEX	Shoaling	1.07	0.55	0.52	0.56	0.58	**0.47**
EROSIVE	Breaking	2.66	2.55	2.09	2.71	**1.74**	2.13
	Inner surf	0.29	0.13	0.17	**0.09**	0.20	0.25
CROSSTEX	Shoaling	0.92	0.68	0.60	0.72	**0.51**	0.58
ACCRETIVE	Breaking	1.09	1.33	1.57	1.65	1.40	**0.39**
	Inner surf	3.03	2.48	2.11	2.79	**1.81**	2.30
LIP	Shoaling	0.29	0.24	0.24	0.29	0.16	**0.05**
EROSIVE	Breaking	1.89	0.49	**0.26**	0.67	0.47	0.85
	Inner surf	0.67	1.03	1.02	1.25	0.76	**0.35**
LIP	Shoaling	0.15	0.08	**0.07**	0.07	0.08	0.13
ACCRETIVE	Breaking	0.33	0.18	0.17	**0.16**	0.20	0.27
	Inner surf	0.11	0.10	0.14	0.14	0.10	**0.03**

595 Note: RMSE is averaged for each cross-shore location, shown in Figs. 1-5, 7. The lowest

596 RMSE values are in **bold and underlined** for convenience.

597

598 **Table 4** - RMSE for each model over all cross-shore regions for each dataset (kg/m^3).

			EROSIVE	ACCRETIVE	EROSIVE	ACCRETIVE
	SINBAD	**SandT-Pro**	**CROSSTEX**	**CROSSTEX**	**LIP**	**LIP**
R39	0.99	1.33	1.66	1.93	1.15	0.22
SR93	2.18	1.76	1.51	1.67	0.66	0.13
LK01	2.10	1.51	1.25	1.56	0.61	0.13
JS07	2.83	1.93	1.60	1.92	0.82	0.13
W12	1.49	0.88	**1.07**	**1.35**	0.52	**0.13**
L19	**0.38**	**0.57**	1.27	1.39	**0.52**	0.17

599 Note: RMSE was taken for all data points (regardless of test case or cross-shore location of
600 measurement) for each dataset in Table, as opposed to taking RMSE for individual test
601 cases/cross-shore locations in Table 2. The lowest RMSE values are highlighted in **bold and**
602 **underlined** for convenience.

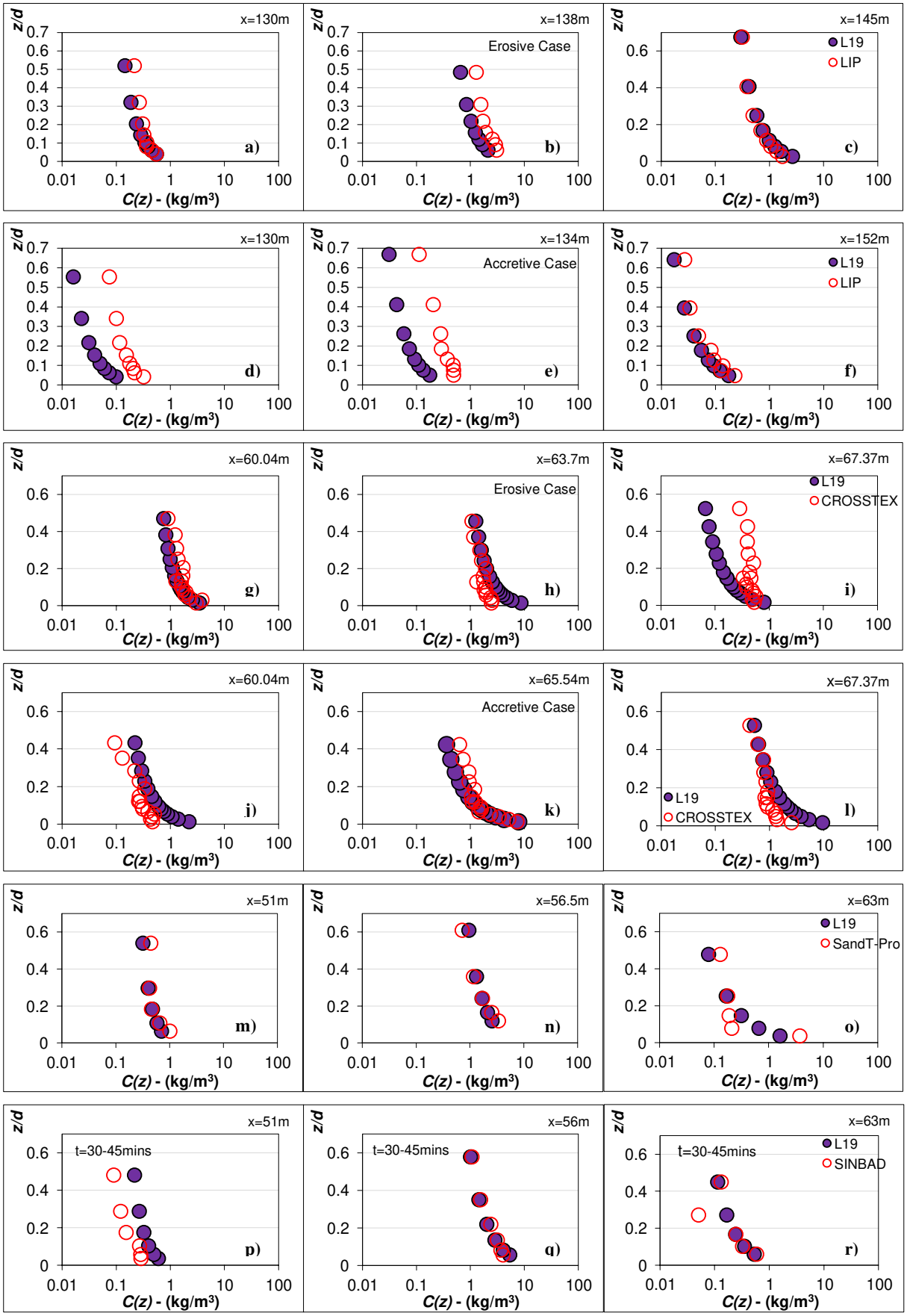


Figure 7 - Concentration profile ($C(z)$) of Measured vs. computed (L19) concentration with new constant $B = 3.3$.

603

604 Plots a-c show LIP erosive, and d-f show LIP accretive cases, respectively. Plots g-i show
605 CROSSTEX erosive and j-l show CROSSTEX accretive cases, respectively. Plots m-o show
606 SandT-Pro and plots p-r are SINBAD. Each row of plots shows three different cross-shore
607 locations: before the breaking point (left plots), at the breaking or plunging point (central plots)
608 and onshore of the breaking point (right plots).

609 Reviewing the performance of all the models tested in this section, the L19 model produces the
610 best results of the power function *C(s)* models and the W12 model produces the best results of
611 the exponential *C(s)* formulae. Comparing the performance of the parabolic L19 concentration
612 profile against the exponential *C(s)* model of W12 in Fig. 8 shows that both models perform
613 very well in almost all cases, with each of the models indicating some small discrepancies in
614 different regions. When analysed qualitatively, the parabolic L19 model generally better
615 mirrors the curved measured concentration profile throughout the whole water column than the
616 W12 model. This is also supported by the RMSE values shown in Table 2, where the L19
617 model has lower (better) RMSE values than the W12 model in 11/18 test cases (RMSE for
618 W12 ranged between 0.08-2.47 kg/m^3, with an average of 0.75 kg/m^3).

619 The W12 model also generally models the measured profile well, but there are some instances
620 where the SSC at the top of the water column and nearest the bed is well-modelled, but not in
621 the mid-water column – this is best demonstrated in Figs. 8f, o, r. This is a result of the quasi-
622 linear concentration profile that essentially serves as a line of best-fit, as discussed under the
623 Larson & Kraus (2001) and Wang et al. (2012) subsections (section 5.4. and 5.6. respectively).
624 Though these discrepancies in the mid-water column are found in most plots, the discrepancies
625 are often negligible. Overall, however, the L19 model is relatively simpler (computationally)
626 and produces slightly better agreement with measured data based on the tests covered in this
627 paper. The implications of the better agreement in *C(s)* on the resulting computed suspended
628 sand transport rates are investigated in a separate related study by the authors.

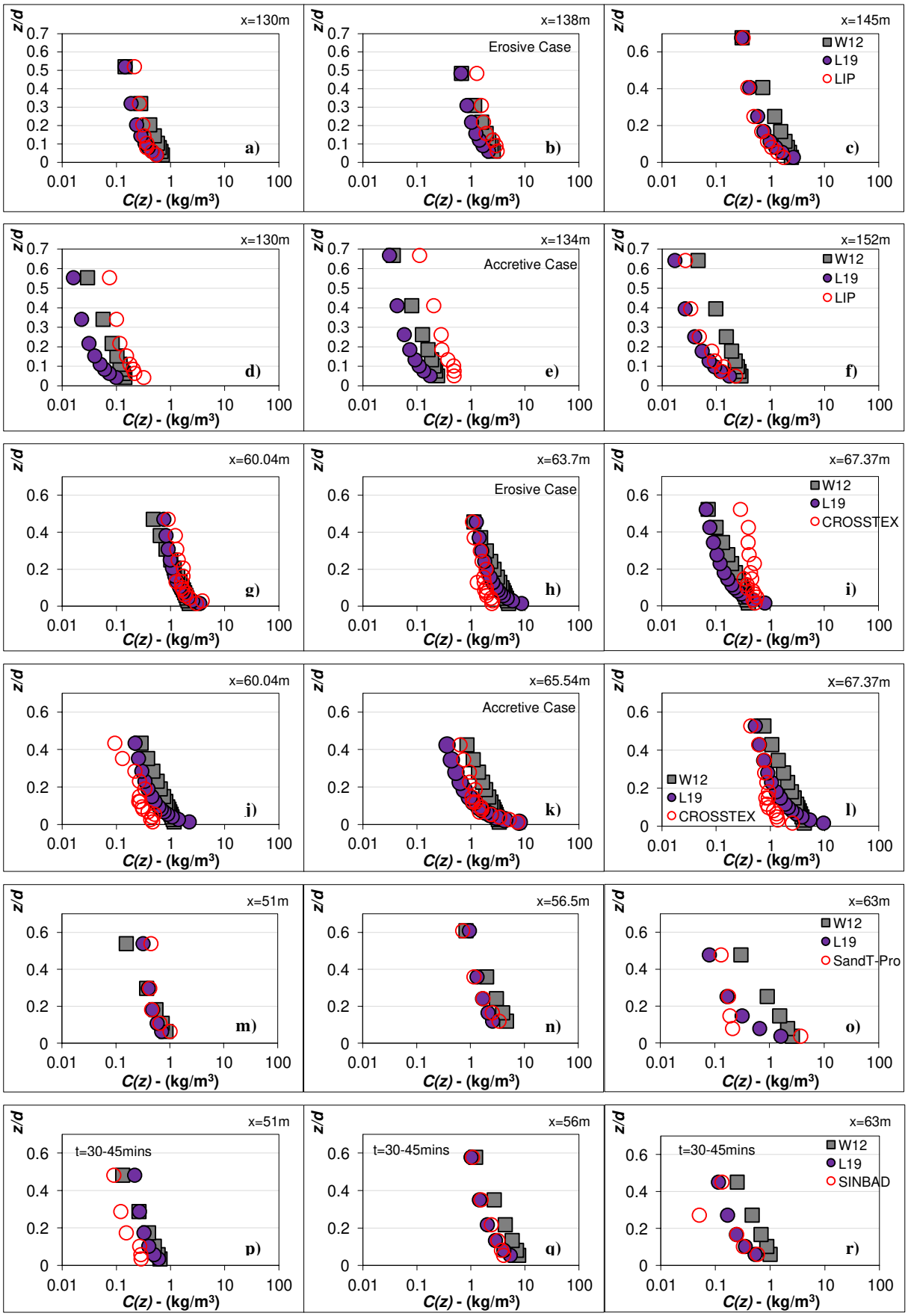


Figure 8 - Concentration profile (*C[z]*) of Measured (red circles) vs. computed (L19, purple circles; W12 grey squares).

629

Plots a-c show LIP erosive and d-f show LIP accretive cases respectively; plots g-i show CROSSTEX erosive and j-l show CROSSTEX accretive cases respectively; plots m-o show are SandT-Pro and plots p-r are SINBAD. Each row of plots shows three different cross-shore locations: before the breaking point (left plots), at the breaking or plunging point (central plots) and onshore of the breaking point (right plots).

The results highlight the limitations of existing profile models under breaking-wave conditions. While none of the tested formulations perfectly captured the vertical distribution across all datasets, the analysis demonstrates where particular approaches succeed or fail: Rouse-type profiles provide reasonable near-bed fits, exponential profiles capture rapid upper decay, and power-law forms offer flexibility but tend to overpredict higher in the water column. The proposed modification in this study represents a first step in this direction. Therefore, the proposed C(s) model has been used in a cross-shore beach profile evolution model described in section 5.8.

5.8. Application of Proposed Modified *C(s)* Model

The applicability of the proposed *C(s)* model was verified through a process-based cross-shore beach profile model, as described in the following subsection. The cross-shore beach profile model was validated using field data collected at the Hasaki Oceanographic Research Station (HORS), Japan. HORS has a long history of coastal measurements (Tabasi et al., 2024), including cross-shore beach profile surveys. The station is equipped with a 427 m-long pier, which has been used for cross-shore beach profile measurements since 1986. From 1986 to March 2011, measurements were conducted daily, while from April 2011 to the present, they have been carried out on a weekly basis.

In this study, beach profiles measured during a storm event from November 5 to 12, 2024 were selected for numerical simulation. Wave data for the simulation were obtained from the

NOWPHAS system, specifically from the Kashima Port buoy, which is the closest available wave measurement station to HORS.

5.8.1. Model Description

The process-based cross-shore beach profile model consists of hydrodynamic, sediment transport, and bed evolution modules, similar to other morphological models. The hydrodynamic calculations, including wave height transformation, were performed using Airy wave theory and the shallow water equations, covering wave propagation from offshore to the swash zone. Since different formulations are required before and after wave breaking, the accurate estimation of the breaking point is crucial and was treated as a calibration parameter. In this study, a breaker index of 0.78, as suggested in several previous studies, was found to be appropriate.

To estimate sediment concentration, the L19 model was employed, and the sediment transport rate was determined accordingly. The diffusion coefficient was computed using diffusion equation given in Lim et al. (2020). The suspended sediment transport rate was estimated as the product of the L19 sediment concentration and the time-averaged current velocity. The total sediment transport rate was obtained as the sum of the suspended sediment transport rate and the bed load transport rate, calculated using an equation proposed by Watanabe (1982). Finally, the bed level change was estimated based on the mass conservation equation as follows:

$$\frac{\partial z_b}{\partial t} + \frac{1}{1-p}\left(\frac{\partial q_x}{\partial x}\right) = 0 \qquad (9)$$

where z_b is the bed level, ∂t the time step for simulation, p the porosity, q_x the sediment transport rate, and x the cross-shore distance.

5.8.2. Model Performance

The model performance was evaluated using the Brier Skill Score (BSS) (similar to Tabasi et al., 2020).

$$BSS = 1 - \frac{\sum(|Z_m - Z_s|)^2}{\sum(|Z_m - Z_i|)^2} \qquad (10)$$

where Z_m is the bed elevation after erosion and formation, Z_s the final simulated bed elevation, and Z_i the initial bed level. Figure 9 presents the simulation results. The initial beach profile, measured on November 5, 2024, corresponded to storm conditions, with a significant wave height of 2.5 m and a wave period of 8 s. Using the L19 concentration model, a BSS of 0.72 was achieved, indicating that the model performance falls within the "good" range.

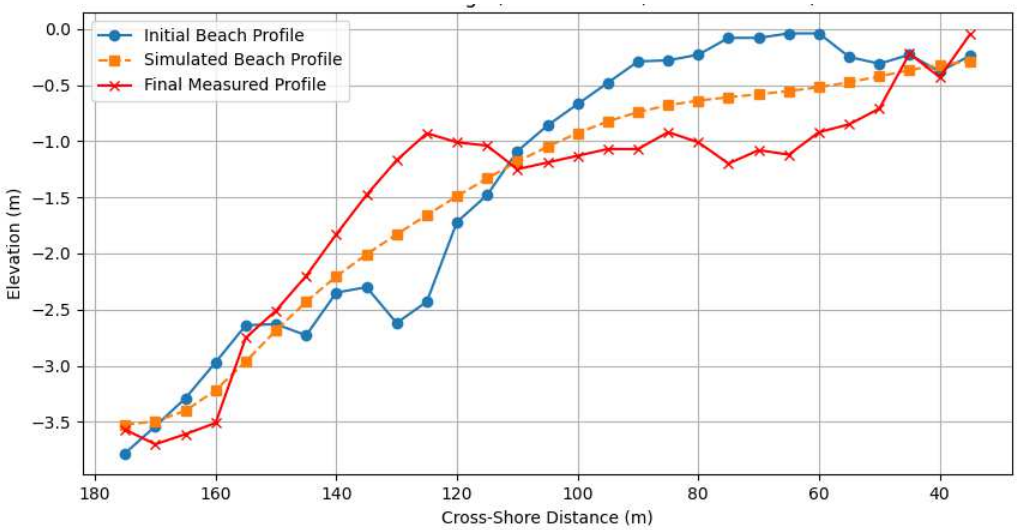


Figure 9 – Comparison between simulated and measured cross-shore beach profiles.

6. Conclusions

In this study, five existing concentration profile (*C(s)*) models were validated against four state-of-the-art laboratory datasets collected under large-scale regular and irregular breaking wave conditions. Existing *C(s)* models were generally separated into two categories: exponential and power-law models. The exponential *C(s)* models produced quasi-linear profiles on the log-scale, practically serving as a line-of-best-fit through the measured concentration profile. As

692 measured profiles were generally parabolic (concave upward shaped), the quasi-linear profiles
693 of the exponential models often did not accurately replicate the shape of the measured
694 concentration profile, instead indicating relatively good agreement in the upper and lower water
695 columns (top and bottom of concentration profile respectively) but showing significant
696 discrepancies in the mid-water column. As suspended flux and transport rate computations are
697 depth-averaged, large discrepancies in the mid-water column can lead to inaccurate estimations
698 of the flux and transport rates. Although all *C(s)* forms depend on C_0, the exponential profiles
699 are especially sensitive since C_0 sets their baseline. Analysis of the various existing *C(s)*
700 formulations were carried out with the base C_0 estimation being made using the L19 C_0 model,
701 which indicated best agreement with measured data. Consequently, the aforementioned
702 discrepancies found in the mid-water column for the exponential *C(s)* models were relatively
703 small. Unlike the previous study by Lim et al. (2020) that focused on reference concentration
704 models, the present work zeroes in on the vertical concentration profile itself and introduces a
705 modified profile formula (with constant B) to better capture SSC distributions.

706 The power function *C(s)* formulae produced parabolic concentration profiles that better
707 reflected the measured profiles. However, the power function formulae were found to be
708 especially sensitive to the magnitude of the dimensionless mixing parameter *M*, which is a
709 function of the balance between sediment entraining and settling forces. Both power function
710 *C(s)* models tested in this paper produced very steep (quasi-linear; vertical) concentration
711 profiles, indicating good agreement in the lower water column (where near-bed agreement was
712 dependent on the reference concentration estimation) but poor agreement in the upper water
713 column. The steep profiles produced by the power function formulae were attributed to the
714 magnitude of *M* being too small. It was proposed that by increasing the overall magnitude of
715 the mixing parameter, a smoother parabolic concentration profile shape could be obtained to
716 better represent the measured profile. This hypothesis was tested in the modified *C(s)* model

(referred to as L19 *C(s)* model), by increasing the magnitude of *M*. The modified L19 profile (with increased M) consistently gave the best fit to observed profiles across zones.

The existing SR93 model was modified to increase the magnitude of the dimensionless mixing parameter (*M*) by incorporating a constant (*B*) to it. The constant *B* was calibrated against a few test cases from the aforementioned datasets. The small addition of the constant improved the performance of the *C(s)* model drastically, indicating that the concentration profile was highly sensitive to mixing parameter (which is usually modelled after the well-known Rouse Number). The modified *C(s)* formula produced significantly improved predictions of the concentration profile, compared to both the original (unmodified) SR93 *C(s)* model and also the alternative existing *C(s)* models. The L19 concentration profile was more gradual than the original (unmodified) SR93 *C(s)* model, showing good agreement with measured *C(s)* throughout the whole water column in all cross-shore zones. The drastic improvement and consistency of good agreement over the majority of test cases suggests that the physical processes accounted for in the power function formulae well-represent the forces in nature. The validation of the proposed *C(s)* model using a process-based cross-shore beach profile model demonstrated its capability to reproduce beach profile changes under storm conditions. Comparison with field measurements from HORS, Japan, showed good agreement, with a Brier Skill Score (BSS) of 0.72, confirming the model's reliability in simulating sediment transport and morphological evolution. The integration of the L19 sediment concentration model and an appropriate breaker index improved the model's predictive accuracy. These findings highlight the potential of the *C(s)* model for coastal engineering applications, particularly in forecasting beach profile evolution under extreme wave conditions.

Acknowledgements

Early parts of this work were supported by the University of East London (UEL) under the UEL's Excellence PhD Studentships Scheme 2017-18. The authors would like to acknowledge Professor Tomoya Shibayama and Waseda University as collaborators in this project. The authors would also like to thank Dr. Joep Van der Zanden of the Maritime Research Institute Netherlands, Professor Daniel Cox of Oregon State University, Professor Hyun Doug Yoon of Myongji University, and Professor Ad Reniers of Delft University of Technology for sharing their datasets with the authors.

Declarations

Ethics Approval

Not applicable. This study did not involve human participants, human data, or animals.

Consent to Participate

Not applicable.

Consent for Publication

Not applicable.

References

Aagaard, T. and Hughes M.G., 2010. Breaker turbulence and sediment suspension in the surf zone. Marine Geology 271, 250-259.

Barbaro, G., Malara, G., Martino, M.C., and Arena, F., 2010. Analytical development of a one-line model for the analysis of shoreline change by wind generated waves. The Open Ocean Engineering Journal, 3, 108-115.

Brand, E., De Sloover, L., De Wulf, A., Montreuil, A.L., Vos, S. and Chen, M., 2019. Cross-Shore Suspended Sediment Transport in Relation to Topographic Changes in the Intertidal Zone of a Macro-Tidal Beach (Mariakerke, Belgium). Journal of Marine Science and Engineering, 7(6), 172.

Brand, E., Montreuil, A.L., Houthuys, R., and Chen, M., 2020. Relating hydrodynamic forcing and topographic response for tide-dominated sandy beaches. Journal of Marine Science and Engineering, 8, 151.

766 Brinkkemper, J.A., Lanckriett, T., Grasso, F., Puleo, J.A. and Ruessink, B.G., 2016. Observations of turbulence
767 within the surf and swash zone of a field-scale sandy laboratory beach. Coastal Engineering 113, 62-72.

768 Camenen, B. and Larson, M., 2008. A general formula for non-cohesive suspended sediment transport. Journal
769 of Coastal Research 24(3), 615-627.

770 Christensen, D.F., Brinkkemper, J., Ruessink, G. and Aagaard, T., 2019. Field observations of intra-wave
771 sediment suspension and transport in the intertidal and shallow subtidal zones. Marine Geology 413, Elsevier,
772 10-26.

773 Dabees, M., and Kamphuis, J.W., 1998. Oneline, a numerical model for shoreline change. Proceedings of 26th
774 International Conference on Coastal Engineering, 2668-2681.

775 Dally, W.R., Dean, R.G., Dalrymple, R.A., 1985. Wave height variation across beaches of arbitrary profile.
776 Journal of Geophysical Research, Oceans, 90.

777 Dam, G., van der Wegen, M., Labeur, R.J., and Roelvink, D., 2016. Modeling centuries of estuarine
778 morphodynamics in the Western Scheldt estuary, Geophysical Research Letters, 43, 3839–3847,

779 Dastgheib, A., 2012. Long-term process-based morphological modeling of large tidal basins. Ph.D. Thesis, IHE
780 Delft and Delft University of Technology, Delft, The Netherlands.

781 Dean, R.G., 1977. Equilibrium beach profiles: U.S. Atlantic and Gulf Coasts. Ocean Engineering Report No. 12,
782 Department of Civil Engineering, University of Delaware, Newark, DE.

783 Dronen, N., and Deigaard, R., 2007. Quasi-three-dimensional modelling of the morphology of longshore bars.
784 Coastal Engineering 54, 197-215.

785 Elias, E., Teske, R., van der Spek, A. and Lazar, M., 2015. Modelling tidal-inlet morphodynamics on medium
786 time scales. Proceedings of the Coastal Sediments 2015, San Diego, California, USA.

787 Fernandez-Mora, A., Ribberink, J.S., van der Zanden, J., van der Werf, J.J., and Jacobsen, N.G., 2016. RANS-
788 VOF modelling of hydrodynamics and sand transport under full-scale non-breaking and breaking waves.
789 Proceedings of the 35th Conference on Coastal Engineering. Antalya, Turkey.

790 Fromant, G., Hurther, D., van der Zanden, J., Van der A, D.A., Cáceres, I., O'Donoghue, T., and Ribberink, J.S.,
791 2019. Wave boundary layer hydrodynamics and sheet flow properties under large-scale plunging-type breaking
792 waves. Journal of Geophysical Research: Oceans, 124.

793 Hanson, H., and Kraus, N.C., 2004. Advancements in One-Line Modeling of T-Head Groins: GENESIS-T.
794 Journal of Coastal Research, Special Issue 33, 315-323

795 Hsu, T.J., and Liu, P.L.F., 2004. Toward modelling turbulent suspension of sand in the nearshore. Journal of
796 Geophysical Research: Oceans, 109(C6).

797 Jayaratne, M.P.R. and Shibayama, T., 2007. Suspended sediment concentration on beaches under three different
798 mechanisms. Coastal Engineering Journal, 49(04), 357-392.

799 Jayaratne, R., Abimbola, A., Balasubramaniam, N., & Tabasi, M. (2025). Numerical modelling of tsunami-
800 induced scour around a coastal dike. *Results in Engineering*, 27, 106557.
801 https://doi.org/10.1016/j.rineng.2025.106557

802 Jayaratne, R., Takayama, Y. and Shibayama, T., 2012. Applicability of suspended sediment concentration
803 formulae to large-scale beach morphological changes. Proceedings of 33rd International Conference on Coastal
804 Engineering, 1(33).

805 Johnson, C.L.; McFall, B.C.; Krafft, D.R.; Brown, M.E., 2021. Sediment Transport and Morphological
806 Response to Nearshore Nourishment Projects on Wave-Dominated Coasts. Journal of Marine Science and
807 Engineering, 9, 1182. https://doi.org/10.3390/jmse9111182

808 Karunarathna, H., Horrillo-Caraballo, J.M. and Reeve, D.E., 2012. Prediction of cross-shore beach profile
809 evolution using a diffusion type model. Continental Shelf Research, 48, 157-166.

810 Karunarathna, H., Horrillo-Caraballo, J.M., Burningham, H., Pan, S., and Reeve, D.E., 2016. Two-dimensional
811 reduced-physics model to describe historic morphodynamic behaviour of an estuary inlet. Marine Geology 382,
812 200-209.

813 Karunarathna, H., Horrillo-Caraballo, J.M., Spivack, M., and Reeve, D.E., 2011. Analysis of key parameters in
814 a diffusion type beach profile evolution model. Continental Shelf Research, 31, 98-107.

815 Klonaris, G.T., Memos, C.D., Drønen, N.K. and Deigaard, R., 2018. Simulating 2DH coastal morphodynamics
816 with a Boussinesq-type model, Coastal Engineering Journal.

817 Kriebel, D.L., Kraus, N.C., and Larson, M., 1991. Engineering methods for predicting beach profile response.
818 Proceedings of Coastal Sediments '91, Reston, VA, 557-571

819 Larson, M., Kraus, N.C., 2001. Estimation of suspended sediment trapping ratio for channel infilling and
820 bypassing. Coastal Engineering Technical Note CETN-IV-34. U.S. Army Engineer Research and Development
821 Center, Vicksburg, Mississippi, 9.

822 Lesser, G.R., Roelvink, J.A., van Kester, J.A.T.M., Stelling, G.S., 2004. Development and validation of a three-
823 dimensional morphological model. Coastal Engineering 51 (8-9), 883-915.

824 Li, M., Fernando, P.T., Pan, S., O'Connor, B.A. and Chen, D., 2007. Development of a quasi-3d numerical
825 model for sediment transport prediction in the coastal region. Journal of Hydro-environment Research 1, 143-
826 156.

827 Lim, G., 2021. Modelling suspended sand transport under breaking waves. Ph.D Thesis, University of East
828 London, London, UK.

829 Lim, G., Jayaratne, R. and Shibayama, T. 2020: Suspended Sand Concentration Models under Breaking Waves:
830 Evaluation of New and Existing Formulations. Marine Geology 426, 106197.

831 Liu, J.H., Yang, S.L., Zhu, Q., and Zhang, J., 2014. Controls on suspended sediment concentration profiles in
832 the shallow and turbid Yangtze Estuary. Continental Shelf Research, 90, 96-108.

833 Luijendijk, A.P., de Schipper, M.A. and Ranasinghe, R., 2019. Morphodynamic acceleration techniques for
834 multi-timescale predictions of complex sandy interventions. Journal of Marine Science and Engineering, 7, 78.

835 Mocke, G.P., and Smith, G.G., 1992. Wave breaker turbulence as a mechanism for sediment suspension.
836 Proceedings of the 23rd International Conference on Coastal Engineering, Venice, Italy.

837 Nielsen, P., 1986. Suspended Sediment Concentrations under Waves. Coastal Engineering, 10(1), 23-31.

838 Nielsen, P., 1992. Coastal Bottom Boundary Layers and Sediment Transport. Singapore: World Scientific, 324.

839 Ogston, A.S. and Sternberg, R.W., 2002. Effect of wave breaking on sediment eddy diffusivity, suspended
840 sediment and longshore sediment flux profiles in the surf zone. Continental Shelf Research 22(4): 633-655.

841 Okayasu, A., 1989. Characteristics of Turbulence Structure and Undertow in Surf Zone, Ph.D Dissertation,
842 University of Tokyo, 53-112.

843 Okayasu, A., Fujii, K., & Isobe, M. 2010. Effect of external turbulence on sediment pickup rate. Proceedings of
844 the 32nd International Conference on Coastal Engineering.

845 Putzar, B. and Malcherek, A., 2014. Modelling of Sediment Transport and Morphodynamics. Die Kuste 81, 89-
846 106.

847 Rattanapitikon, W., and Shibayama, T., 1998. Energy dissipation model for regular and irregular breaking
848 waves, Coastal Engineering Journal, 40(4), 327–346.

849 Ribberink, J., Van der A, D., Van der Zanden, J., O'Donoghue, T., Hurther, D., Cáceres, I. and Thorne, P., 2014.
850 Sandt-Pro: Sediment transport measurements under irregular and breaking waves, Proceedings of 34th
851 Conference on Coastal Engineering, 1(34).

852 Roelvink, J.A., Reniers, A.J.H.M., 1995. LIP 11D Delta Flume experiments, A data set for profile model
853 validation. Report H2130, Delft Hydraulics, The Netherlands.

854 Rouse, H., 1939. Experiments on the Mechanics of Sediment Suspension. Proceedings of the 5th International
855 Congress for Applied Mechanics. New York, 550-554.

Sanchez, A., Brown, M., Beck, T., Styles, R. and Li, H., 2015. Long-term morphological modeling at Coastal inlets. Proceedings of the Coastal Sediments 2015, San Diego, California, USA.

Sato, S., Homma, K. and Shibayama, T., 1990. Laboratory study on sand suspension due breaking waves. Coastal Engineering in Japan, 33(2), 219–231.

Schepper, R.; Almar, R.; Bergsma, E.; de Vries, S.; Reniers, A.; Davidson, M.; Splinter, K., 2021. Modelling Cross-Shore Shoreline Change on Multiple Timescales and Their Interactions. Journal of Marine Science and Engineering, 9, 582. https://doi.org/10.3390/jmse9060582

Scott, C. P., Cox, D.T., Maddux, T.B. and Long, J.W., 2005. Large-scale laboratory observations of turbulence on a fixed barred beach. Measurement Science and Technology 16(10): 1903-1912.

Shibayama, T., and Rattanapitikon, W., 1993. Vertical distribution of suspended sediment concentration in and outside surf zone. Coastal Engineering in Japan, 36(1), 49–65.

Smith, G.G., & Mocke, G.P. 1993. Sediment suspension by turbulence in the surf zone. Proceeding of Euromech 1993, Le Havre, France.

Spielmann, K., Astruc, D., & Thual, O. 2004. Analysis of some key parametrizations in a beach profile morphodynamical model. Coastal Engineering, 51(10), 1021-1049.

Sun, Z., Zheng, H., Xu, D., Hu, C., and Zhang, C., 2020. Vertical concentration profile of non-uniform sediment. International Journal of Sediment Research.

Svendsen, I.A. 1984. Wave Heights and Setup in a Surf-zone. Coastal Engineering 8, 303-329.

Tabasi, M., Soltanpour, M., Suzuki, T., Jayaratne, R.M., 2020. Sediment Transport and Modeling of Berm Formation and Erosion at the Southern Coast of the Caspian Sea. Int. Conf. Coastal. Eng., No 36v, papers.19. https://doi.org/10.9753/icce.v36v.papers.19.

Tabasi, M., Suzuki, T., Cox, D.T., Okayasu, A., 2024. Artificial neural network-based model to predict mega cusp characteristics in Hasaki, Japan. Geomorphology. 464, https://doi.org/10.1016/j.geomorph.2024.109377.

Thorne, P. D., Davies, A. G., & Williams, J. J. (2009). Measurements of near-bed intra-wave sediment entrainment above vortex ripples. *Journal of Geophysical Research*, 114.

Thornton, E.B. and Guza, R.T. 1983. Transformation of wave height distribution. Journal of Geophysical Research 88(C10), 5925.

van der A, D. A., van der Zanden, J., O'Donoghue, T., Hurther, D., Cáceres, I., McLelland, S.J. and Ribberink, J.S., 2017. Large-scale laboratory study of breaking wave hydrodynamics over a fixed bar. Journal of Geophysical Research: Oceans, 122, 3287–3310.

van der Wegen, M., and Roelvink, J.A., 2008. Long-term morphodynamic evolution of a tidal embayment using a two-dimensional, process-based model, Journal of Geophysical Research: Oceans, 113, C03016.

van der Werf, J. J., van Veen, R., Ribberink, J. S., & van der Zanden, J. 2015. Testing of the new SANTOSS transport formula in the Delft3D morphological modelling system. Proceedings of the Coastal Sediments 2015, San Diego, USA (1-14).

van der Zanden, J., 2016. Sand transport processes in the surf and swash zones. Ph.D Thesis, University of Twente, Netherlands.

Van der Zanden, J., Fernandez-Mora, A., Van der A, D.A., Hurther, D., Cáceres, I., O'Donoghue, T., and Ribberink, J.S., 2017**c**. Inclusion of wave breaking turbulence in reference concentration models. Proceedings of Coastal Dynamics 2017. Helsingor, Denmark. 14, 629-641.

van der Zanden, J., van der A, D.A., Cáceres, I., Hurther, D., McLelland, S.J., Ribberink, J.S. and O'Donoghue, T., 2018. Near-bed turbulent kinetic energy budget under a large-scale plunging breaking wave over a fixed bar. Journal of Geophysical Research: Oceans, 123,

van der Zanden, J., van der A, D.A., Cáceres, I., Larsen, B.E., Fromant, G., Petrotta, C., Scandura, P., and Li, M., 2019. Spatial and temporal distributions of turbulence under bichromatic breaking waves. Coastal Engineering, 146, 65-80.

van der Zanden, J., van der A, D.A., Hurther, D., Cáceres, I., O'Donoghue, T., and Ribberink, J.S., 2016. Near-bed hydrodynamics and turbulence below a large-scale plunging breaking wave over a mobile barred bed profile. Journal of Geophysical Research: Oceans, 121(8), 6482-6506.

van der Zanden, J., van der A, D.A., Hurther, D., Cáceres, I., O'Donoghue, T., Hulscher, S.J.M.H. and Ribberink, J.S., 2017**a**. Bedload and suspended load contributions to breaker bar morphodynamics. Coastal Engineering, 129, 74–92.

van der Zanden, J., van der A, D.A., Hurther, D., Cáceres, I., O'Donoghue, T., and Ribberink, J.S. 2017**b**. Suspended sediment transport around a large-scale laboratory breaker bar. Coastal Engineering, 125, 51–69.

van Rijn, L. C., 1993. Principles of sediment transport in rivers, estuaries and coastal seas. The Netherlands: Aqua Publications, 831.

van Rijn, L.C., 1984. Sediment Transport, Part II: Suspended Load Transport. Journal of Hydraulic Engineering, 110(11), 1613-1641.

van Rijn, L.C., 2007. Unified View of Sediment Transport by Currents and Waves. II: Suspended Transport. Journal of Hydraulic Engineering, 133(6), 668-689.

van Rijn, L.C., Ribberink, J.S., van der Werf, J., and Walstra, D.J.R., 2013. Coastal sediment dynamics: recent advances and future research needs. Journal of Hydraulic Research 51(5): 475-493.

Wang, L., Zimmermann, N., Trouw, K., de Maerschalck, B. and Vanlede, J., 2014. Numerical modelling of long-term morphology in the surf zone of the Belgian coast. Proceedings of the International Conference on Coastal Engineering, 1(34).

Wang, P., Yuan, W., Min, L., 2012. Measuring and modelling suspended sediment concentration profiles in the surf zone. Journal of Palaeogeography, 1(2), 172-193.

Wang, P., Smith, E. R., Ebersole, B. A., 2002. Large-scale laboratory measurements of longshore sediment transport under spilling and plunging breakers. Journal of Coastal Research, 18: 118-135.

Yoon, H.D. and Cox, D.T., 2010. Large-scale laboratory observations of wave breaking turbulence over an evolving beach. Journal of Geophysical Research: Oceans 115(C10).